Appl. Phys. B 49, 397–407

Applied Physics B Photophysics and Laser Chemistry

Two Unstable Oscillations in the Multimode Laser with Modulated Inversion

Tetsuo Ogawa

Department of Applied Physics, Faculty of Engineering, The University of Tokyo, 7-3-1 Hongo, Bunkyo-ku, Tokyo 113, Japan

Received 27 April 1989/Accepted 17 July 1989

Abstract. We present comprehensive results of numerical studies on the dynamical properties of a multimode ring laser under modulation of the population inversion in the bad-cavity condition. Incoherent properties of unstable oscillations in this system are investigated in detail as a function of two control parameters: the dc component of the population inversion and the modulation amplitude. Two kinds of optical chaos in two limiting regions reported in a previous paper are extensively studied to clarify their different characteristics from deterministic and stochastic points of view. The competition between their different origins is revealed. Statistical properties of their stochasticity are investigated to clarify their *non-Gaussian* natures. Comparison with analytical results for a single-mode laser with fluctuations is also made.

PACS: 42.50.Tj, 42.55.−f, 05.45.+b

The theoretical understanding of the dynamical properties of lasers as dissipative nonlinear dynamical systems far from thermal equilibrium is relatively advanced. This has provided a basis for describing an irregular asymptotic evolution as deterministic chaos [1, 2]. On the other hand, the spectral and temporal characteristics of lasers have also attracted interest of researchers in engineering and experimental fields: Ultra-high time resolution spectroscopy with temporally incoherent laser light has been developed [3–6]. The well-controlled optical chaos appears to be a candidate for an incoherent light source. Detailed information on the characteristics of the incoherent light is essential for the analysis of incoherent laser spectroscopy. In addition, we need to control the temporal coherency of laser light for various purposes. The quality control of the laser light has potential applications in many fields.

Because the simplest model of a laser system with a few degrees of freedom is that of a single-mode unidirectional ring laser under cw pumping, this model has already been investigated extensively [2]. The multimode and/or modulated (nonautonomous) lasers, however, are still far from a full understanding with respect to their coherence and dynamical characteristics. The coupled nonlinear equations which describe the operation of a multimode system are too complicated to be solved generally. Nevertheless, the multimode and/or modulated lasers are important from both the engineering and fundamental viewpoints, and are essential in obtaining ultrashort light pulses under the mode-locked operation. In addition, it is also interesting to clarify the relation between two kinds of optical chaos corresponding to the modulated and unmodulated systems, which are a characteristic of the nonequilibrium nonlinear system.

The dynamics of lasers is characterized by three relaxation constants: the field decay rate K including a transmission loss through the cavity mirrors, the polarization (transverse) relaxation constant $\gamma_\perp$ and the population (longitudinal) relaxation constant $\gamma_\parallel$. According to a linear stability analysis [7, 8] of the mean-field Maxwell-Bloch equations, the stability of cw laser operation depends on these constants: cw oscillation can be unstable under the bad-cavity (low-Q cavity) condition ($K > \gamma_\parallel + \gamma_\perp$), while stable

under the good-cavity (high-Q cavity) condition ($K < \gamma_{\parallel} + \gamma_{\perp}$). In this paper, we pay attention to the former case to clarify the unstable phenomena.

In our previous papers [9,10], we employed the technique of population inversion modulation in a multimode system as a method for controlling the coherence. There we introduced the regular and chaotic behavior of this system and their dependence on physical parameters. The modulation of the atomic inversion of a multimode ring laser induces large qualitative changes in the stability properties of its output laser field, depending sensitively also on the cavity Q-value (inversely proportional to K). In the case of a bad cavity (low-Q cavity, $K \gg \gamma_{\parallel}, \gamma_{\perp}$), an important feature was that optical chaos was observed in two limiting cases [10]: first, when the dc component of inversion is very large, and second, when the modulation is fairly strong but the dc component is weak. Chaos in the first region results from the intrinsic Lorenz instability [11], which occurs even in the case of no modulation. On the other hand, the second region of chaos is essentially caused by the strong modulation, where the mechanism has also been investigated in the single-mode laser with a low-Q cavity [12,13].[1] These types of chaos coexist in a parameter space of the multimode system.

The aim of this paper is to show that above two kinds of chaos have different characteristics with respect to ergodic and statistical properties. In particular, the correlation dimensions of their chaotic attractors show a distinct difference. The competition between the different origins of instabilities in the multimode system, i.e., the Lorenz-type instability and the quasiperiodic instability, is also revealed for the first time. The former instability overcomes the latter in the large population inversion even under strong modulation. We also perform dimensional analysis and discuss the validity of the calculations in [10]. Moreover, we stress that the total electric field of both two kinds of chaos does not obey the complex Gaussian random process. Several characteristics that differ in the two cases are investigated from a statistical point of view. A distribution function of the electric field amplitude with a long tail is obtained in the strong pumping region, which was also predicted by an analytical study of the Fokker-Planck equation of the bad-cavity laser [14]. The main results of this paper are summarized as follows.

1) Two unstable oscillations of the multimode laser with modulated inversion in the bad-cavity condition are studied to clarify their differences in terms of ergodic and stochastic natures. The competition between two types of chaos originating in different instabilities is investigated: The quasiperiodic instability is suppressed by the Lorenz instability in the region of the large inversion.

2) The optical chaos in the limiting region of large population inversion (LC) has the following properties: a) The correlation dimensions of attractors of the field amplitude are about 2.07 ± 0.06–2.21 ± 0.06. b) The power spectral density of the field has a very broad profile and a power tail in frequency. c) The static probability distribution of the field amplitude has a long tail and is well characterized by the F-type distribution. Higher order statistical moments deviate from those calculated from the complex Gaussian statistics.

3) The other type of optical chaos observed in the region of strong modulation and lower population inversion (QPC) is characterized by following facts: a) The correlation dimensions of attractors of the field amplitude are about 2.34 ± 0.06–2.50 ± 0.06. b) The power spectrum is exponential-like. c) The static probability density of the field amplitude is well described by a Γ distribution.

4) The correlation dimensions of the chaotic attractor are calculated as a function of the sampling time interval (resolution time) to test the validity of the dimensional calculation of [10].

In Sect. 1, a general theoretical model for a multimode ring laser with population inversion modulation is reviewed. In Sect. 2, we survey the different characteristics of the two kinds of chaos in ergodic and statistical terms. The plausibility of the correlation dimension is discussed there. Non-Gaussian statistical properties are also revealed. A discussion is presented in Sect. 3.

1. Multimode Laser Equation of Motion

Conventional laser theory is based upon *two* coupled rate equations for the light intensity and the population difference obtained after adiabatic elimination of the atomic polarization. This treatment is not justified in our bad-cavity case where the Lorenz instability comes from *three* coupled differential equations. Moreover, phase dynamics are increasing in importance, not only in terms of fundamental interests, but also due to recent developments in optical communication and optical information processing [15]. Therefore, neither the adiabatic approximation nor the rate-equation treatment are justified in both the good- and bad-cavity cases. We must treat the coupled equations for the radiation field, the atomic polar-

[1] The interaction between the longitudinal modes in a low-Q cavity is destructive and noncooperative. In the good-cavity system, on the other hand, strong modulation leads to a coherent pulsation, i.e., mode-locking phenomena [9]. This results from a cooperative interaction between the modes. This is an essential difference between these two systems from a phenomenological point of view

ization, and the population difference in an exact manner without any adiabatic eliminations.

We study the temporal behavior of a travelling-wave field interacting with a homogeneously broadened medium under sinusoidal modulation of the population inversion in a unidirectional ring cavity [10]. The active medium consists of the two-level atoms with the relaxation constants $\gamma_\perp$ and $\gamma_\parallel$ for the polarization and population, respectively. The interaction of the active atoms with the cavity field is described by the travelling-wave Maxwell-Bloch equations:

$$\left[c\frac{\partial}{\partial z}+\frac{\partial}{\partial t}\right]E(z,t)=-\kappa E+igP, \tag{1.1a}$$

$$\frac{\partial}{\partial t}P(z,t)=-\gamma_\perp P+i\Delta_A P-igED, \tag{1.1b}$$

$$\frac{\partial}{\partial t}D(z,t)=-\gamma_\parallel D+\gamma_\parallel D^{(0)}+\gamma_\parallel\zeta\cos\omega_m t+2ig[EP^*-E^*P], \tag{1.1c}$$

where E is the complex total field envelope, P the atomic polarization envelope, and D the population difference. Here, κ is the decay rate of the field in the medium, Δ_A the detuning of the carrier frequency of the field from the central atomic transition frequency, and g is the coupling constant. The population inversion is sinusoidally modulated from outside with the modulation frequency ω_m and amplitude ζ around its dc component $D^{(0)}$. Here, ω_m is chosen to be close to the longitudinal mode spacing $2\pi c/L$ of the cavity with the length L chosen to give not only the temporally incoherent light but also the coherent mode-locked laser pulsation [16]. Consequently, the side modes as well as the central mode of the population difference are excited and they are coupled with each other through the nonlinear intermode interaction. This induces coupling between the adjacent modes of the electric field.

Equations (1.1) are supplemented by the boundary condition of the unidirectional ring cavity:

$$E(0,t)=RE(\ell,t-\Delta t)\exp(-i\delta_c), \tag{1.2}$$

where R is the mirror reflectivity, ℓ the length of gain medium, and δ_c the phase difference due to cavity detuning. Δt is the delay time due to round trip: $\Delta t=(L-\ell)/c$. Taking into account the spatial dependence according to the boundary condition (1.2), the lasing threshold is given by

$$D_{th}=\left(\frac{\kappa\gamma_\perp}{g^2}+\frac{c\gamma_\perp}{\ell g^2}|\ln R|\right)\left(1+\frac{\Delta_A^2}{\gamma_\perp^2}\right)\equiv\frac{L}{\ell}\frac{K\gamma_\perp}{g^2}\left(1+\frac{\Delta_A^2}{\gamma_\perp^2}\right), \tag{1.3}$$

where K is an effective field relaxation constant including transmission losses through the cavity mirrors.

With the aid of the "dressed-mode" transformation [10, 28], the boundary condition for the field (1.2) is reduced to a simpler *periodic* form. In addition, due to the spatial mode decomposition, we can eliminate the spatial differential $\partial/\partial z$ to obtain multimode laser equations in a natural manner. As a result, an infinite set of coupled *ordinary* differential equations are obtained for the mode-decomposed variables.[2] In this paper, we confine ourselves to the case of $\Delta_A=\delta_c=0$. Then we can obtain the Maxwell-Bloch equations for the mode-decomposed components as

$$\frac{d}{dt}e_n(t)=-Ke_n-in\Delta_m e_n+ig\frac{\ell}{L}p_n, \tag{1.4a}$$

$$\frac{d}{dt}p_n(t)=-\gamma_\perp p_n+in\omega_m p_n-ig\sum_k\sum_l\xi_{kln}e_k d_l\times\exp[-i(k+l-n)\omega_m t], \tag{1.4b}$$

$$\frac{d}{dt}d_n(t)=-\gamma_\parallel d_n+in\omega_m d_n+\gamma_\parallel\eta_n D^{(0)}\exp(in\omega_m t)+\gamma_\parallel\Delta_n\frac{\zeta}{2}\exp[i(n-1)\omega_m t]+2ig\sum_k(e_k p^*_{k-n}-e^*_k p_{k+n}),\quad (n=0,1,2,\ldots), \tag{1.4c}$$

where

$$\xi_{kln}=\frac{1-R^2}{R^2}\frac{1}{2|\ln R|+2\pi i(k+l-n)}, \tag{1.5a}$$

$$\eta_n=\frac{1-R^2}{2|\ln R|+2n\pi i}, \tag{1.5b}$$

$$\Delta_n=\frac{1-R^2\exp(i\omega_m\Delta t)}{2|\ln R|+i(2n\pi-\omega_m\Delta t)}, \tag{1.5c}$$

$$\Delta_m=\frac{2\pi c}{L}-\omega_m. \tag{1.5d}$$

Equation (1.4c) has the source term for the $(n-1)$th mode component of the population difference (the fourth term of the right hand side of the equation) due to the pumping modulation whose frequency is close to the mode spacing. This is an essential difference from the models of [28, 29] where a free-running operation is considered. The efficiency of the modulation is

[2] Although the transformed electric field always satisfies the periodic boundary condition, the transformed polarization and population do not. Nevertheless, we employ the spatial Fourier expansion for them by assuming their periodic nature. Therefore, we should pay attention to the fact that the solutions of the multimode equations lie only in a *subspace* of those of the original Maxwell-Bloch equations

measured by the coefficient A_n given by (1.5c). Here note that $d_n(t)=d^*_{-n}(t)$ because of the real-valued nature of the population difference. These multimode equations contain the rigorous form of the cavity boundary condition (1.2) describing the propagation of the field. We stress again that our relevant model (1.4) has been derived without the uniform-field approximation. Spatial dependencies of these variables are described through the expansions in terms of the spatial eigenmodes. Their temporal characteristics are followed through the time development of the expansion coefficients in addition to the Fourier components. Thus we can obtain reliable and exact information about the temporal evolution of this system by using this model (1.4).

The Maxwell-Bloch equations in the mode-decomposed forms (1.4) are useful when a small number of modes are operating simultaneously. Here, we need to pay attention to the fact that the number of relevant modes should be nearly equal to the ratio of the power-broadened atomic linewidth to an intermode spacing. That linewidth is described by the larger of the unsaturated gain width $2\gamma_\perp$ and the Rabi frequency $g(\gamma_\perp/\gamma_\parallel)^{1/2}|E|$.

2. Characteristics of the Two Types of Optical Chaos

Let us study in this section how the external modulation influences a multimode system which has an intrinsic instability even without the modulation. The bad-cavity condition ($K>\gamma_\parallel,\gamma_\perp$) has been achieved experimentally by the far-infrared (FIR) laser (e.g., NH_3 laser, CH_2F_2 laser) or the molecular electronic transition laser (e.g., I_2 laser) to observe the Lorenz instability in recent experiments [30–32]. Because the modulation of the population inversion and the multimode operation were shown to be effective in reducing the threshold for chaos [10], the chaotic behavior of the modulated multimode laser with a bad cavity will be more easily observed. The other kind of chaos, i.e., a quasiperiodic chaos, at low static population inversion but at higher modulation amplitude is also observable.

For numerical calculation, we choose such a case, since the active frequency region of gain is covered by the five modes $n=0, \pm1, \pm2$. For the population difference d_n, however, additional population pulsation terms [28] $d_{\pm3}$ and $d_{\pm4}$ are considered to allow more precise analysis. As a result, the 29-dimensional coupled differential equations (1.4) are integrated with a fourth-order Runge-Kutta-Gill routine which avoids the accumulation of rounding-off errors. We choose $K=10.0\gamma_\perp$, $\gamma_\parallel=0.5\gamma_\perp$, $R=0.2$, $g=4.35$, $\ell/L=2.7\times10^{-3}$, $2\pi c/L=0.51\gamma_\perp$, and $\Delta_m=0$. We vary $D^{(0)}$ and ζ as the two control parameters. The field amplitude is

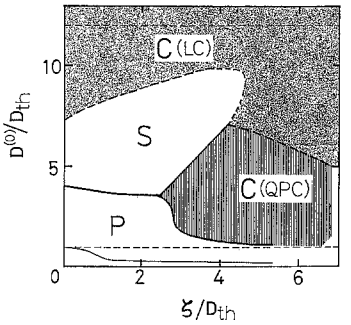

Fig. 1. Phase diagram of the modulation characteristics in the space of the dc component of the population inversion $D^{(0)}$ and the modulation amplitude ζ under $K=10.0\gamma_\perp$, $\gamma_\parallel=0.5\gamma_\perp$, $R=0.2$, and $\Delta_m=0.0$. Chaos due to the Lorenz instability (LC) are observed in upper dark C region. In the lower black C region, the system shows quasiperiodic chaos (QPC). The upper horizontal broken line represents the instability threshold D^B_{th}. Thick broken lines denote ambiguous boundaries. This phase diagram is coarse grained, and a realistic diagram is filled with finer structure of quasiperiodic and periodic chaos, phase-locking, etc.

normalized by its steady-state value $|E^S(z=0)|$ whose intensity is given by

$$|E^S(0)|^2=\frac{\gamma_\perp\gamma_\parallel}{4g^2}\left(\frac{D^{(0)}}{D_{th}}-1\right)\left(1+\frac{\Delta_A^2}{\gamma_\perp^2}\right)\frac{R\sinh(\Theta-|\ln R|)}{\sinh\Theta}, \quad (2.1)$$

where

$$\Theta=\left(\frac{\ell}{c}\kappa+|\ln R|\right)\left(1-\frac{D_c}{D^{(0)}}\right), \quad (2.2a)$$

$$D_c=\frac{\kappa\gamma_\perp}{g^2}\left(1+\frac{\Delta_A^2}{\gamma_\perp^2}\right). \quad (2.2b)$$

Here we briefly review the modulation responses of this system found in [10]. The dynamic characteristics are classified in the parameter space of $D^{(0)}$ and ζ, as shown schematically in Fig. 1. Roughly speaking, this space can be divided into three regions, S, P, and C, based upon the power spectrum profile, the phase space trajectory, and the time evolution of the amplitude and phase. The S region is located at weak modulation and intermediate population inversion, in which the laser system shows stable cw emission or emission with slight modulation. In this region, the phase of the total field varies almost linearly and slowly in time. The P region has a rich dynamics including the periodic pulsation, the aperiodic pulsation, the stable quasiperiodic oscillation, the unstable quasiperiodic oscillation, and so on. Detailed studies of these phenomena are presented in [10].

2.1. The Two Kinds of Optical Chaos

When $D^{(0)}$ and/or ζ are fairly large, this multimode system shows irregular dynamics as optical chaos in the regions denoted by C. This response is in contrast

to the case of the good-cavity system [9, 10], which exhibits a coherent train of pulses in the limit of large modulation amplitude ζ. In order to classify in more detail the dynamical characteristics of the C region, we employ the dimensionality test, calculating the correlation dimensions [33, 34] of the attractors of the chaotic field amplitude. According to the dimensional analysis discussed in the next subsection, the C region can be further divided into two regions. One (LC) is located at the region of very high $D^{(0)}$ and the other (QPC) at rather low $D^{(0)}$ and fairly strong modulation (high ζ), as shown in the phase diagram (Fig. 1). The chaos observed in the region of high $D^{(0)}$ (LC) has the same origin as the Lorenz instability. The resonant mode is described by the Lorenz equations, so this mode loses its stability in the high $D^{(0)}$ situation [11]. On the other hand, chaotic behavior (QPC) in the region of rather low $D^{(0)}$ and very strong modulation (high ζ) results from the quasiperiodic instability [35] in which the external modulation plays an essential role [13]. The boundary line between the two regions of chaos is approximately found as

$$D^{(0)}+\zeta \simeq D_{\mathrm{th}}^{\mathrm{B}} \equiv \left\{5+3\frac{\gamma_{\parallel}}{\gamma_{\perp}} +2\left[4+6\frac{\gamma_{\parallel}}{\gamma_{\perp}}+2\left(\frac{\gamma_{\parallel}}{\gamma_{\perp}}\right)^2\right]^{1/2}\right\} D_{\mathrm{th}}, \tag{2.3}$$

This means that as long as the maximum peaks of the modulated population inversion exceed the instability threshold $D_{\mathrm{th}}^{\mathrm{B}}$, the chaotic behavior originates from the Lorenz instability. Thus the Lorenz instability suppresses the quasiperiodic instability in the high $D^{(0)}$ region. Therefore the quasiperiodic chaos can be observed only in the lower $D^{(0)}$ and high ζ region. So we conclude that these instabilities compete exclusively with each other. The quantitative differences between these types of chaos are presented below.

Here it should be noted that the phase motions of these two kinds of chaos observed in both LC and QPC regions behave very randomly, in contrast to the "stable" phase motion of the Lorenz chaos observed in the single-mode bad-cavity laser [29, 36, 37]. This may stem from the multimode property of the mode-mode couplings. This point is one of the characteristic features of chaos in the multimode system.

2.2. *Correlation Dimensions of the Attractors*

Strong evidence for the difference in origins between LC and QPC chaos is given by dimensional analysis. Here we concentrate on the correlation dimension, using the method proposed by Grassberger and Procaccia [33, 34]. We start with a series of data $u(1), u(2), \ldots, u(i), \ldots$ in a time sequence, corresponding to measurements regularly spaced in time where time is discretized by a sampling (resolution) time interval Δt as $t=i\Delta t$ $(i=1,2,\ldots)$. From the $u(i)$'s, a sequence of points $\mathbf{x}(1), \mathbf{x}(2), \ldots$, is obtained by taking

$$\mathbf{x}(i)=[u(i), \ldots, u(i+d-1)],$$

a d-dimensional vector. We use this sequence $\mathbf{x}(1), \mathbf{x}(2), \ldots, \mathbf{x}(N)$ to constitute the correlation integral $C^{(d)}(\varepsilon)$ as follows:

$$C^{(d)}(\varepsilon)=\frac{1}{N^2}\{\text{number of pairs } [\mathbf{x}(i), \mathbf{x}(j)] \text{ such that } \|\mathbf{x}(i)-\mathbf{x}(j)\| \leqq \varepsilon\}. \tag{2.4}$$

Here, d is the embedding dimension and $\|\mathbf{x}-\mathbf{x}'\|$ is the Euclidean norm of $\mathbf{x}-\mathbf{x}'$. Suppose now that

$$\lim_{\varepsilon \to 0} \lim_{N \to \infty} \frac{\log C^{(d)}(\varepsilon)}{\log \varepsilon} = D_2^{(d)}. \tag{2.5}$$

For d sufficiently large, $D_2 \equiv \lim_{d \to \infty} D_2^{(d)}$ is the correlation dimension. We have calculated the D_2 dimensions of the attractors formed by the *amplitude* of the chaotic fields, i.e., $u(i)=|E(i)|$.

Although the effects of the temporal resolution of the time series Δt and the number of data points N upon the correlation dimension are discussed by several authors [38–40], they are not yet understood in detail from the fundamental and theoretical points of view. Therefore, we have calculated the dimensions in several time intervals Δt between data points, as shown in Fig. 2a. From this figure, one observes a dependence of D_2 on the sampling time interval. In the case of too small Δt, D_2 becomes less than two. The values in plateau regions are the correct ones [41]. The inhomogeneity or non-uniformity of the strange attractor of a system with many degrees of freedom [42] like the multimode laser may be reflected in the fact that the correlation dimension is less than or near two. A strongly dissipative character of this system is also reflected in the small D_2.

The correlation dimensions of the strange attractors in each of the two limiting regions (LC and QPC) are found to be fractional and, to within ± 0.06 error, are 2.07–2.21 for LC and 2.34–2.50 for QPC. A fractional dimension indicates that the observed field behavior is "chaotic". Moreover, the convergence of $D_2^{(d)}$ for sufficiently large d is evidence that the chaotic fields do not have stochastic origins. The clear difference in D_2 between LC and QPC comes from the different origins of the chaos. Figure 2b shows the $D^{(0)}$ dependence of the correlation dimension D_2 in the case of the rather strong modulation amplitude ($\zeta/D_{\mathrm{th}} \simeq 3.0$–$6.0$). Two different dimensions exist: the higher dimensions (○) are found in the lower $D^{(0)}$ and the lower dimension (●) in the high $D^{(0)}$. This indicates that the Lorenz instability (●) suppresses the quasiperiodic instability (○) even in the strong modulation case if $D^{(0)}$ is large.

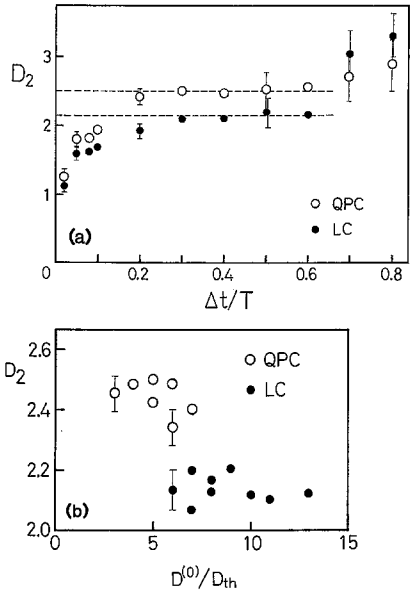

Fig. 2. **a** The correlation dimension D_2 of the chaotic field amplitude as a function of the sampling time interval Δt for the cases of $D^{(0)}/D=11.0$, $\zeta/D_{th}=0.0$ (denoted by •) and $D^{(0)}/D_{th}=5.0$, $\zeta/D_{th}=4.5$ (denoted by o). The total number of data points is fixed at 3000 and T denotes a characteristic time of the dynamics (the correlation time). The broken lines stand for the values in plateau regions. **b** The correlation dimension D_2 plotted against the dc population inversion $D^{(0)}$ under the relatively strong modulation condition, i.e., $\zeta/D_{th}=3.0$–6.0. The higher dimension (o) is observed in the lower $D^{(0)}$ corresponding to quasiperiodic chaos (QPC), and the lower dimension (•) in the higher $D^{(0)}$ corresponds to Lorenz-type chaos (LC)

2.3. Routes to Chaos

The abrupt transition to LC chaos from cw emission (S region) is analogous to the case of Lorenz chaos. As shown in the phase diagram, this chaotic region also exists below the threshold $D_{th}^{B}\sim 12.0D_{th}$. In terms of obtaining temporally incoherent light in experiments, the multimode operation has the advantage of reducing the instability threshold. On the other hand, the characteristic route to QPC chaos can be observed as a function of the modulation amplitude ζ with fixed lower population inversion $D^{(0)}$. When the modulation amplitude is small in the region P, the system exhibits a periodic pulsation whose frequency coincides with the external modulation frequency (harmonic oscillation). On increasing the modulation amplitude, another quasiperiodic frequency incommensurate to the modulation frequency grows, and stable quasiperiodic oscillation occurs after the subcritical Neimark bifurcation [12, 13, 35]. This quasiperiodic motion forms a torus in phase space. This torus structure collapses to yield an *unstable* quasiperiodic behavior at stronger modulation. These two incommensurate frequencies, i.e., the harmonic oscillation frequency and the induced quasiperiodic one compete with each other resulting in an intermittent behavior with these two frequencies irregularly superposed. Finally, dynamical structure with several frequencies changes into completely irregular chaotic behavior which is the fully developed chaos. The nonlinear coupling between the modes corresponding to the different frequencies tends to destroy quasiperiodicity and replace it by chaos according to the Ruelle-Takens-Newhouse theorem [46,47].

2.4. Power Spectral Densities and Intensity Autocorrelation Functions

Figures 3a and b show the power spectra of the chaotic (LC) field observed in the high $D^{(0)}$ limit on a semi-logarithmic and a log-log-scale, respectively. We find

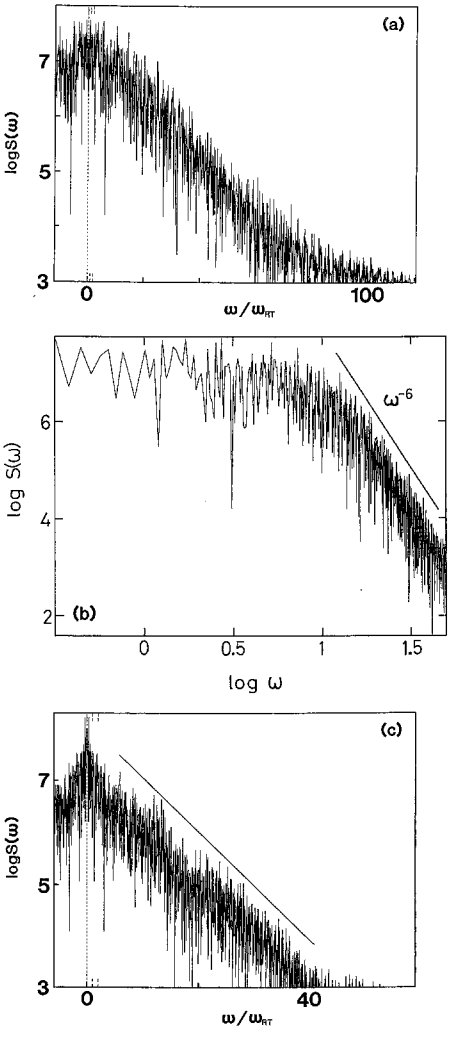

Fig. 3a–c. Power spectral density of the field in the high $D^{(0)}$ region **a** in the semi-log frame and **b** in the log-log frame for $D^{(0)}/D_{th}=14.0$ and $\zeta/D_{th}=0.0$. The tail shows the power decay. The frequency is measured by $\omega_{RT}=2\pi c/L$. **c** In the low $D^{(0)}$ and high ζ region (QPC) in the semi-log frame for $D^{(0)}/D_{th}=4.0$ and $\zeta/D_{th}=3.5$

that the power spectrum of LC chaos has a very broad profile with a power tail. This indicates that there is no characteristic scale of frequency in the power regions of the spectrum. On the other hand, the spectrum of the other kind of chaos (QPC) at low $D^{(0)}$ and high ζ is shown in Fig. 3c on semi-log scale. In this plot, the spectrum profile is found to have an exponential dependence on the frequency ω. Thus the power spectra of the chaotic fields in both limiting regions distinct differences.

The intensity autocorrelation function $C^{(2)}$ is a measure of the second order coherence of the emitted light, defined as

$$C^{(2)}(\Delta\tau)=\frac{\langle E^*(t)E^*(t+\Delta\tau)E(t+\Delta\tau)E(t)\rangle}{\langle E^*(t)E(t)\rangle^2}. \tag{2.6}$$

In both regions, $C^{(2)}(\Delta\tau)$ decays rapidly as a function of the time difference $\Delta\tau$ and shows no correlation peaks at the time difference corresponding to the round-trip time (Fig. 4a and 4b). This results in a small correlation time which is further evidence of the incoherence of the chaotic light. If the total field obeys the complex Gaussian random process, the intensity autocorrelation function $C^{(2)}$ can be written in terms of the field correlation

$$C^{(1)}(\Delta t)=\langle E^*(t)E(t+\Delta\tau)\rangle/\langle|E(t)|^2\rangle$$

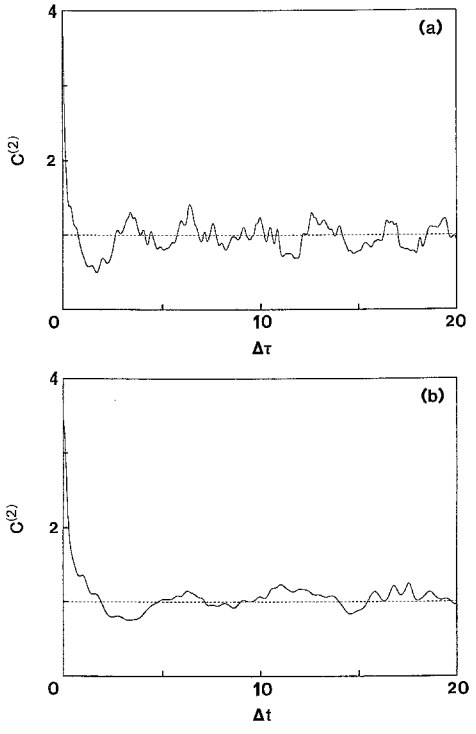

Fig. 4. a The intensity autocorrelation function of the chaotic light in the high $D^{(0)}$ region (LC). The peak value is 3.78. The time difference $\Delta\tau$ is measured by the transverse relaxation time $\gamma_\perp^{-1}$. **b** In the low $D^{(0)}$ and high ζ region (QPC). The peak value is 3.47

as

$$C^{(2)}(\Delta\tau)=1+|C^{(1)}(\Delta\tau)|^2, \tag{2.7}$$

using the factorization properties of the higher order moments [48]. Therefore, the ratio of the peak to background in the intensity autocorrelation functions becomes 2:1. In this system, however, the ratios are about 3.78:1 and 3.47:1 in the high $D^{(0)}$ (LC) and high ζ (QPC) cases, respectively. This indicates that the total fields do not obey the simple Gaussian process.

2.5. *Static Probability Distributions of the Field Amplitude*

From the viewpoint of applications, chaotic temporal behavior is sometimes regarded as a stochastic process. We then have another means of distinguishing between the origins of LC and QPC chaos as well as the deviation of these statistics from the Gaussian type.

The density distribution of the chaotic fields are shown in Fig. 5a–c. In the region of high $D^{(0)}$ and low ζ (LC), the probability density (Fig. 5a) of the amplitude of the field can be fitted by a power-tailed distribution function (F-type distribution):

$$W(|E|)\propto|E|^{\alpha-1}\left[1+\varepsilon\frac{\alpha}{\beta}|E|^2\right]^{-(\alpha+\beta+1)} \quad \text{for LC}, \tag{2.8}$$

where α and β are positive constants related to the strengths of fluctuations, and ε is also a positive parameter, to be discussed in Sect. 3. On the other hand, the distribution function in the low $D^{(0)}$ and high ζ (QPC) region (Fig. 5b) can be well described as a special case of a Γ distribution:

$$W(|E|)=a^2|E|\exp(-a|E|) \quad \text{for QPC}, \tag{2.9}$$

with a positive parameter a. Both functions have profiles different from the Rayleigh (Wigner) distribution resulting from the complex Gaussian statistics introduced in the appendix.

In each of the two regions, the probability distribution of the phase is almost uniform with the value of $1/2\pi$, as shown in Fig. 5c. This comes from the superposition of the complex fields of the multimodes which obey the chaotic motions. However, the residual singular structure (seen as δ-function-like spikes) retains traces of the characteristic property of chaos as a "dynamical system".

2.6. *Higher Order Moments*

Here we present a second example of deviation of the chaotic fields from the Gaussian statistics. The higher order moments reflect more strongly the tail structure of the probability distribution [49]. The skewness α_3^E

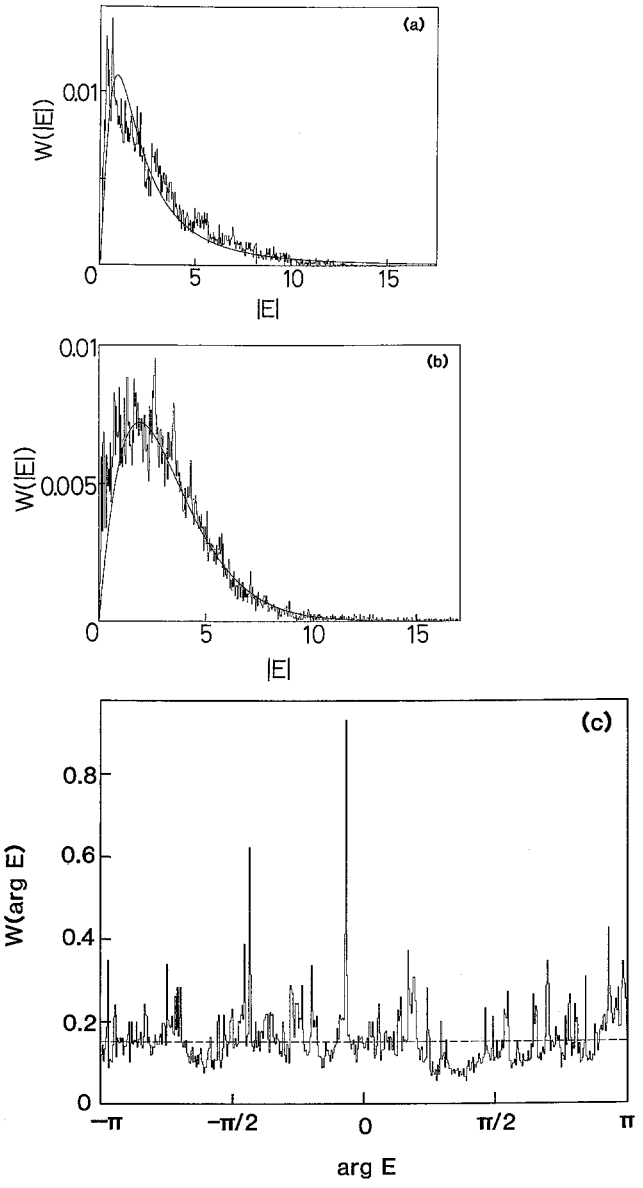

Fig. 5. a The static probability distribution of the amplitude of chaos **a** in the high $D^{(0)}$ region (LC) and **b** in the low $D^{(0)}$ and high ζ region (QPC). The fitted solid lines are the F-type distribution (2.8) and the Γ distribution (2.9), respectively. **c** The probability distribution of the phase of total field of LC chaos. The broken line is the uniform distribution $1/2\pi$

and the flatness α_4^E of the amplitude distribution are calculated from time series data. These are shown in Table I where the different values from the Gaussian case are shown. In the limit of high ζ (QPC), the skewness and the flatness are evaluated as 1.40 and $3+3.01$, respectively, as shown in Table 1. These values coincide well with that calculated from the fitting probability density assuming the Γ distribution (2.9): $\alpha_3^E=\sqrt{2}$ and $\alpha_4^E=3+3$. The fact that both α_3^E and α_4^E are larger than 0.631 and $3+0.245$, respectively, is a result of the longer tail of the amplitude distribution than that of a Rayleigh distribution.

Table 1. Typical values of the skewness and flatness of the total field amplitude of the optical chaos observed in two limiting regions. The number of datapoints is 2^{15}

	Skewness α_3^E	Flatness α_4^E
LC	1.41	$3+4.32$
QPC	1.40	$3+3.01$
Rayleigh	0.631	$3+0.245$

Table 2. The normalized intensity moments of the chaotic light observed in the high $D^{(0)}$ limit (LC) for the bad-cavity case. The number of datapoints is 2^{15}. Compare with the values $n!$ in the case of the complex Gaussian light. Diverging values for large n result from the long-tailed distribution

Order n	2	3	4	5	6
Chaotic	3.783	26.92	324.1	4771.8	77490.7
Gaussian	2	6	24	120	720

A further proof of the long-tail property is given by the nth order normalized intensity moments $m_{\text{int}}(n)$:

$$m_{\text{int}}(n)\equiv\frac{\langle(E^*E)^n\rangle}{\langle E^*E\rangle^n},\quad (n=2,3,\ldots). \tag{2.10}$$

Table 2 shows the diverging intensity moments as a function of the order n. These indicate the longer tail of the probability distribution compared to that of the complex Gaussian statistics. The second-order normalized intensity moment $m_{\text{int}}(2)$ is connected to the photon counting coefficient,

$$\eta\equiv m_{\text{int}}(2)-1=\langle n^2\rangle/\langle n\rangle^2-\langle n\rangle^{-1}-1,$$

where n is the number of photoelectrons in the photon counting experiment. For Bose-Einstein statistics (corresponding to ℓ complex Gaussian case), η becomes unity, whereas for Poisson statistics (in the case of coherent light), η is zero. In our calculation, η is larger than two. Therefore, the optical chaos has incoherence with strange statistical properties.

2.7. *Cross-Correlation Coefficients*

In order to confirm that the real and the imaginary parts of the electric field are not correlated, the cross-correlation coefficient $K(0)$ is a good measure of the cross-correlation defined as

$$K(0)=\frac{\langle[\text{Re}\{E(t)\}-\langle\text{Re}\{E\}\rangle][\text{Im}\{E(t)\}-\langle\text{Im}\{E\}\rangle]\rangle}{\sqrt{\sigma_R^2}\sqrt{\sigma_I^2}}, \tag{2.11}$$

where σ_R^2 and σ_I^2 are the variances of the real and imaginary parts of the field, respectively. The correlation coefficients are calculated as about -0.063 (LC) and -0.128 (QPC) in the high $D^{(0)}$ and the high ζ regions, respectively. This means that the correlation between the $\mathrm{Re}\{E\}$ and $\mathrm{Im}\{E\}$ is almost negligible. Thus we conclude that they are not statistically correlated.

3. Discussion

A problem to be solved is the dependence of the number of modes upon the coherence of emitted field. Depending on this number, we must use an appropriate model to describe the laser. 1) In single-mode operation, a laser becomes a low-dimensional system if fluctuations are negligible. 2) When several longitudinal modes oscillate as in the present case, the system has many degrees of freedom particularly if the three relaxation constants are of the same order. Here numerical analysis is a suitable method for studying the high-dimensional properties. 3) When infinitely many modes operate simultaneously, as in a dye laser, stochastic forces may be employed to describe the fluctuation effects of the off-resonant modes on the relevant resonant mode [50, 51]. From a naive viewpoint, the system in which a great number of modes operate independently and simultaneously is epxected to emit random light with Gaussian statistics because of the central limit theorem. On the other hand, the single-mode system is not stochastic but fully dynamical. The system of a few modes discussed in this paper has an intermediate character between the dynamical and the stochastic system. It should be noted that the central limit theorem cannot be applied to the multimode laser system because modes are not independent of one another and the mode-mode interaction plays an important role in the laser dynamics [52–55].

In view of the above discussion, we studied the statistical properties of the bad-cavity laser emission with the aid of the Langevin and the Fokker-Planck equations. In the case of strong pumping ($D^{(0)} \gg D_{\mathrm{th}}$), the bad-cavity laser is equivalent to the stochastic Toda oscillator whose statistical properties are described by the Kramers-like equation. According to [14], the normalized light intensity $\bar{I}=|\bar{E}|^2$ in the cavity, whose mean value is normalized to be $\bar{A} \equiv D^{(0)}/D_{\mathrm{th}}-1$, has a probability distribution with a power tail:

$$W(\bar{I}) \propto \bar{I}^{\gamma\bar{A}/2S_D-1}\left(1+\frac{S_E}{4S_D}\bar{I}\right)^{-(1+2\gamma/S_E+\gamma\bar{A}/2S_D)}, \quad (3.1)$$

where $\gamma=\gamma_{\parallel}/\gamma_{\perp}$, and S_E and S_D are measures of the strength of field (including the off-resonant modes) and population noises, respectively. Therefore, the normalized amplitude of the electric field $|\bar{E}|=\sqrt{\bar{I}}$ also has a power distribution with a tail:

$$W(|\bar{E}|) \propto |\bar{E}|^{\gamma\bar{A}/S_D-1} \times\left(1+\frac{S_E}{4S_D}|\bar{E}|^2\right)^{-(1+2\gamma/S_E+\gamma\bar{A}/2S_D)}. \quad (3.2)$$

These results are valid in the case of $\bar{A}S_E \ll 4S_D$. Normalized intensity moments $m_{\mathrm{int}}(n)$ are calculated from above distribution function as

$$m_{\mathrm{int}}(n)=\left(\frac{4S_D}{\bar{A}S_E}\right)^n B\left(\frac{\gamma\bar{A}}{2S_D}+n,\ 1+\frac{2\gamma}{S_E}-n\right) \times\left[B\left(\frac{\gamma\bar{A}}{2S_D},\ 1+\frac{2\gamma}{S_E}\right)\right]^{-1}, \quad (3.3)$$

for $n<1+2\gamma/S_E$, where $B(x, y)$ is the beta function. The first two moments are explicitly written as

$$m_{\mathrm{int}}(2)=\frac{1+2S_D/\gamma\bar{A}}{1-S_E/2\gamma}, \quad (3.4a)$$

$$m_{\mathrm{int}}(3)=\frac{(1+2S_D/\gamma\bar{A})(1+4S_D/\gamma\bar{A})}{(1-S_E/2\gamma)(1-S_E/\gamma)}. \quad (3.4b)$$

We find that the field fluctuation and the off-resonant mode noise (measured by S_E) play an essential role in a large fluctuation due to the long tail of the distribution function. Increasing the order n, the denominator of $m_{\mathrm{int}}(n)$ becomes small. Therefore, $m_{\mathrm{int}}(n)$ grows more rapidly than the Gaussian case. As shown in Sect. 2.5, this distribution explains well the numerical result of the deterministic multimode laser. Therefore, the stochastic character of LC chaos can also be understood by the Langevin model with the multimode effects replaced by fluctuating forces.

In the strong modulation limit of the bad-cavity case, the quasiperiodic instability induces chaotic behavior (QPC) as shown in the route to chaos. Dynamics of the atomic variables P and D for the resonant mode can be described by the simple equation of the forced Toda oscillator under the very-bad-cavity condition [12]. Analytical studies confirmed that the bad-cavity system with modulation has intrinsically a quasiperiodic mode to generate chaos. These analyses were presented in [12, 13].

Here we mention the Lorenz plot (return map) of the chaotic field amplitude in the bad-cavity case. In neither region of LC or QPC, can we obtain a well-defined transfer function by calculating the Lorenz plot of the amplitude $|E(t)|$, in contrast to the single-mode case [12]. The chaotic dynamics of this multimode system cannot be described by the simple one-dimensional map, in spite of the low correlation dimensions. The character of the continuous time in the differential equations (not a *map*) plays an essential role in generating these kinds of chaos.

For the application of optical chaos to incoherent laser spectroscopy, we need to clarify how the non-Gaussian statistical properties affect the measurement of ultra-fast phenomena. The dependence upon the spectroscopic scheme and the nonlinear optical processes also remains to be clarified. We must choose a laser material in which longitudinal and transverse relaxation constants are of the same order so as to observe this chaotic behavior in experiments. Wide applications can be expected only when continuous control of the cavity quality and of the number of modes has been achieved.

Acknowledgements. The author would like to thank Prof. E. Hanamura, Prof. K. Ikeda (RIFP, Kyoto University), Prof. M. G. Raymer, Dr. N. Nagaosa, Dr. K. Otsuka (NTT), Dr. D. Takahashi, and Dr. M. Tachikawa for fruitful discussions and encouragement. He is also grateful to Prof. N. B. Abraham for sending him valuable comments on the calculation of the correlation dimension. This work has been supported by the Scientific Research Grant-in-Aid from the Ministry of Education, Science, and Culture of Japan.

Appendix

The Complex Gaussian Statistics

When we assume that the complex field $\bar{E}(t)$ obeys the complex Gaussian process, that is, the real and imaginary parts of $\bar{E}$ are independent stochastic variables whose distributions are Gaussian:

$$W(\mathrm{Re}\{\bar{E}\}, \mathrm{Im}\{\bar{E}\}) = \frac{1}{\pi\bar{A}} \exp\left[-\frac{(\mathrm{Re}\{\bar{E}\})^2 + (\mathrm{Im}\{\bar{E}\})^2}{\bar{A}} \right], \quad \text{(A.1)}$$

where $\bar{A}$ is a pumping parameter $\bar{A} \equiv D^{(0)}/D_{\mathrm{th}} - 1$, and $\bar{E}$ is normalized to be $\langle |\bar{E}|^2 \rangle = \bar{A}$. In this case, the amplitude $|\bar{E}|$ and the phase $\arg\{\bar{E}\}$ have the Rayleigh (Wigner) and the uniform distributions, respectively:

$$W(|\bar{E}|) = \frac{2}{\bar{A}} |\bar{E}| \exp\left(-\frac{|\bar{E}|^2}{\bar{A}} \right), \quad |\bar{E}| \geqq 0, \quad \text{(A.2a)}$$

$$W(\arg\{\bar{E}\}) = \frac{1}{2\pi}, \quad 0 \leqq \arg\{\bar{E}\} < 2\pi. \quad \text{(A.2b)}$$

From this, the stationary moments of field amplitude m_n are

$$m_n \equiv \langle |\bar{E}|^n \rangle = \begin{cases} n!!(\pi/2)^{1/2}(\bar{A}/2)^{n/2}, & \text{for } n\text{: odd}, \\ (n/2)!\,\bar{A}^{n/2}, & \text{for } n\text{: even}. \end{cases} \quad \text{(A.3)}$$

The skewness α_3^E and the flatness α_4^E of the amplitude distribution (A.2a) are thus given as

$$\alpha_3^E \equiv \frac{m_3 - 3m_1 m_2 + 2m_1^3}{(m_2 - m_1^2)^{3/2}} = \frac{2(\pi - 3)\sqrt{\pi}}{(4-\pi)^{3/2}} \simeq 0.631, \quad \text{(A.4a)}$$

$$\alpha_4^E \equiv \frac{m_4 - 4m_1 m_3 + 6m_2 m_1^2 - 3m_1^4}{(m_2 - m_1^2)^2} = \frac{32 - 3\pi^2}{(4-\pi)^2} \simeq 3 + 0.245. \quad \text{(A.4b)}$$

The light intensity $\bar{I} \equiv |\bar{E}|^2$ has an exponential distribution defined as

$$W(\bar{I}) = \frac{1}{\bar{A}} \exp\left(-\frac{\bar{I}}{\bar{A}} \right), \quad \bar{I} \geqq 0, \quad \text{(A.5)}$$

whose skewness and flatness are $\alpha_3 = 2$ and $\alpha_4 = 3 + 6$, respectively. The normalized intensity moment $m_{\mathrm{int}}(n)$ is

$$m_{\mathrm{int}}(n) \equiv \frac{m_{2n}}{(m_2)^n} = n!, \quad n = 1, 2, \ldots. \quad \text{(A.6)}$$

References

1. J.-P. Eckmann, D. Ruelle: Rev. Mod. Phys. **57**, 617 (1985)
2. Special issue "Nonlinear Dynamics of Lasers," J. Opt. Soc. Am. B **5**, No. 5 (1988)
3. N. Morita, T. Yajima: Phys. Rev. A **30**, 2525 (1984)
4. R. Beach, D. DeBeer, S.R. Hartmann: Phys. Rev. A **32**, 3467 (1985)
5. S. Asaka, H. Nakatsuka, F. Fujiwara, M. Matsuoka: Phys. Rev. A **29**, 2286 (1984)
6. T. Kobayashi, A. Terasaki, T. Hattori, K. Kurokawa: Appl. Phys. B **47**, 107 (1988)
7. H. Risken, K. Nummedal: J. Appl. Phys. **39**, 4662 (1968)
8. L.A. Lugiato, L.M. Narducci, M.F. Squicciarini: Phys. Rev. A **34**, 3101 (1986)
9. T. Ogawa, E. Hanamura: Opt. Commun. **61**, 49 (1987)
10. T. Ogawa, E. Hanamura: Appl. Phys. B **43**, 139 (1987)
11. E.N. Lorenz: J. Atmos. Sci. **20**, 130 (1963)
12. T. Ogawa: Phys. Rev. A **37**, 4286 (1988)
13. T. Ogawa: Jpn. J. Appl. Phys. **27**, 2292 (1988)
14. T. Ogawa: Phys. Rev. A **39**, 2264 (1989)
15. J.B. Anderson, T. Aulin, C.-E. Sundberg: *Digital Phase Modulation* (Plenum, New York 1986)
16. This situation is different from the cases of [17–27] in which the modulation frequency is much smaller than the longitudinal mode spacing
17. H.J. Scholz, T. Yamada, H. Brand, R. Graham: Phys. Lett. **82A**, 321 (1981)
18. S. Tarucha, K. Otsuka: IEEE J. QE-**17**, 810 (1981)
19. F.T. Arecchi, R. Meucci, G. Puccioni, J. Tredicce: Phys. Rev. Lett. **49**, 1217 (1982)
20. I.I. Matorin, A.S. Pikovskii, Ya.I. Khanin: Sov. J. Quant. Electron. **14**, 1401 (1984)
21. W. Klische, H.R. Telle, C.O. Weiss: Opt. Lett. **9**, 561 (1984)
22. E. Brun, B. Derighetti, D. Meier, R. Holzner, M. Ravani: J. Opt. Soc. Am. B **2**, 156 (1985)
23. Chang-Hee Lee, Tae-Hoon Yoon, Sang-Yung Shin: Appl. Phys. Lett. **46**, 95 (1985)
24. J.R. Tredicce, F.T. Arecchi, G.P. Puccioni, A. Poggi, W. Gadomski: Phys. Rev. A **34**, 2073 (1986)
25. D. Dangoisse, P. Glorieux, D. Hennequin: Phys. Rev. Lett. **57**, 2657 (1986)
26. Dhruba J. Biswas, Vas Dev, U.K. Chatterjee: Phys. Rev. A **35**, 456 (1987)
27. T. Erneux, S.M. Baer, P. Mandel: Phys. Rev. A **35**, 1165 (1987)
28. L.A. Lugiato, L.M. Narducci, E.V. Eschenazi, D.K. Bandy, N.B. Abraham: Phys. Rev. A **32**, 1563 (1985)
29. L.M. Narducci, J.R. Tredicce, L.A. Lugiato, N.B. Abraham, D.K. Bandy: Phys. Rev. A **33**, 1842 (1986)
30. C.O. Weiss: J. Opt. Soc. Am. B **2**, 137 (1985)
31. C.O. Weiss, J. Brock: Phys. Rev. Lett. **57**, 2804 (1986)
32. T.Q. Wu, C.O. Weiss: Opt. Commun. **61**, 337 (1987)
33. P. Grassberger, I. Procaccia: Physica **9D**, 189 (1983)

34. P. Grassberger, I. Procaccia: Physica **13**D, 34 (1984)
35. J.M.T. Thompson, H.B. Stewart: *Nonlinear Dynamics and Chaos* (Wiley, New York 1986)
36. A.C. Fowler, J.D. Gibbon, M.J. McGuinness: Physica **4**D, 139 (1982)
37. C.O. Weiss, N.B. Abraham, U. Hubner: Phys. Rev. Lett. **61**, 1587 (1988)
38. H. Atmanspacher, H. Scheingraber, W. Voges: Phys. Rev. A **37**, 1314 (1988)
39. D.J. Gauthier, P. Narum, R.W. Boyd: Phys. Rev. Lett. **58**, 1640 (1987)
40. J.W. Havstad, C.L. Ehlers: Phys. Rev. A **39**, 845 (1989)
41. N.B. Abraham: Private communication. In our previous paper [10], the D_2's were underestimated to be less than two. This resulted from the inappropriate choice of too small a sampling time interval $\Delta t \simeq T/20$, where T is a correlation time of the dynamics
42. In further investigations, we need to calculate the global spectra $f(\alpha)$ and $h(\lambda)$ to clarify the density distribution of the points in the strange attractors, especially of the high dimensional systems (see [43–45])
43. T.C. Halsey, M.H. Jensen, L.P. Kadanoff, I. Procaccia, B.I. Shraiman: Phys. Rev. A **33**, 1141 (1986)
44. J.-P. Eckmann, I. Procaccia: Phys. Rev. A **34**, 659 (1986)
45. D.J. Gauthier, P. Narum, R.W. Boyd: Technical digest of International Workshop on Instabilities, Dynamics and Chaos in Nonlinear Optical Systems, Italy 1987, pp. 65
46. D. Ruelle, F. Takens: Commun. Math. Phys. **20**, 167 (1971)
47. S.E. Newhouse, D. Ruelle, F. Takens: Commun. Math. Phys. **64**, 35 (1978)
48. For example, R. Loudon: *The Quantum Theory of Light*, 2nd edn. (Clarendon, Oxford 1983)
49. D.S. Broomhead, J.N. Elgin, E. Jakeman, S. Sarkar, S.C. Hawkins, P. Drazin: Opt. Commun. **50**, 56 (1984)
50. T. Ogawa: Appl. Phys. B **48**, 327 (1989)
51. T. Ogawa: IEEE J. QE-**25** (October 1989)
52. H. Atmanspacher, H. Scheingraber: Phys. Rev. A **34**, 253 (1986)
53. L.A. Westling, M.G. Raymer, M.G. Sceats, D.F. Coker: Opt. Commun. **47**, 212 (1983)
54. L.W. Casperson: J. Appl. Phys. **46**, 5194 (1975)
55. F.T. Hioe: J. Math. Phys. **19**, 1307 (1978)